

# VNHC and Acrobot Title

Adan Moran-MacDonald, *Member, IEEE*, Manfredi Maggiore, *Member, IEEE\**, and Xingbo Wang

## Abstract

In this article we study virtual nonholonomic constraints, which are relations between the generalized coordinates and generalized momenta of a mechanical system that can be enforced via feedback control. We design a constraint which emulates gymnastics giant motion in an acrobot, and rigorously prove that this constraint will inject or dissipate energy. This constraint is tested on a real-world acrobot, demonstrating highly effective energy regulation properties and robustness to a variety of disturbances.

## Index Terms

energy regulation, virtual nonholonomic constraints, acrobot, gymnastics.

## I. INTRODUCTION

In gymnastics terminology, a “giant” is the motion a gymnast performs to achieve full rotations around a horizontal bar [1]. A gymnast will begin by hanging at rest, then swing their legs appropriately to gain energy over time. The authors of [2] modelled the gymnast as a variable length pendulum, and studied how the pendulum’s length changes as a function of the gymnast’s limb angle. Labeling the pendulum length by  $r$  and the gymnast’s body orientation by  $\theta$ , they observed experimentally that the value  $\dot{r}/r$  has the biggest impact on the magnitude of energy injection. After testing several gymnasts under a variety of experimental conditions, they discovered that the peak value of  $\dot{r}/r$  occurred at the same fixed value of  $\dot{\theta}/\theta$  for all gymnasts. In other words, gymnasts appear to move their legs as a function of their body angle and velocity when performing giants; doing so allows them to gain energy and rotate around the bar.

While the simplest model of a gymnast is the variable-length pendulum, a more realistic model is the two-link acrobot (Figure 1). Here, the top link represents the torso while the bottom link represents the legs. The acrobot is actuated exclusively at the center joint (the hips). Controlling the acrobot is a nontrivial task because it is not feedback linearizable [3]. To solve the swingup problem, one might begin by designing a leg controller which provably injects energy into the acrobot, so that the resulting motion mimics that of a human performing a giant.

Previous attempts at acrobot giant generation have involved trajectory tracking, partial feedback linearization, or other energy-based methods ( see [5]–[8] ). While all these approaches succeed at making the acrobot rotate around the bar, none of them use the results of [2]. That is, none of these leg controllers track a function of the acrobot’s body angle and velocity. In 2016, Wang attempted to design such a controller [4] but was unable to prove the acrobot would gain energy over time. His approach was a rudimentary version of a recent technique know as the method of virtual nonholonomic constraints.

Manuscript submitted for review on May 14, 2021.

A. Moran-MacDonald (e-mail: adan.moran@mail.utoronto.ca) and M. Maggiore (e-mail: maggiore@control.utoronto.ca) are with the Department of Electrical and Computer Engineering, University of Toronto, ON, Canada.

X. Wang is with ??? (e-mail: ???).

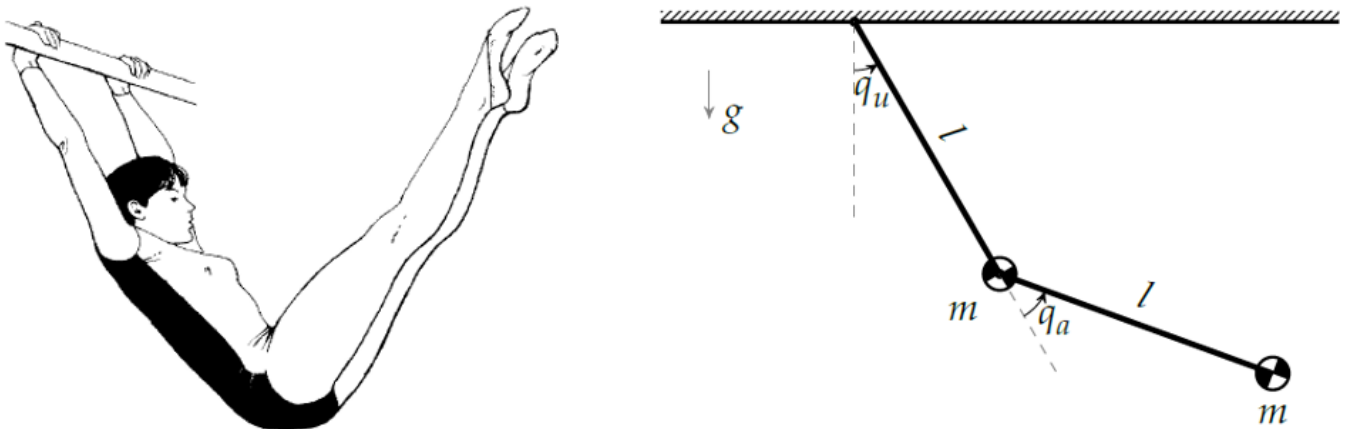


Fig. 1: The two-link acrobot as a model for a gymnast. Image modified from [4].

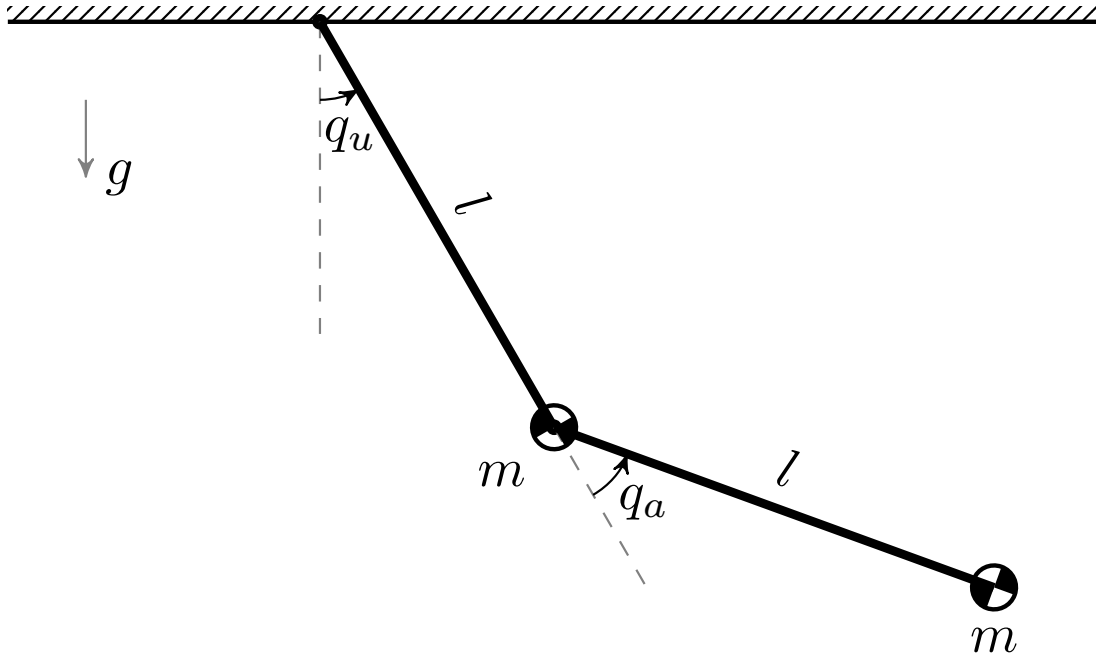


Fig. 2: A simple acrobot has massless rods of equal length  $l$  and equal masses  $m$  at the tips.

Virtual nonholonomic constraints (VNHCs) have been used for human-robot interaction [9]–[11], error-reduction on time-delayed systems [12], and they have shown marked improvements to the field of bipedal locomotion [13]–[15]. Indeed, they produce more robust walking motion in biped robots than other virtual constraints which do not depend on velocity [16]. In particular, VNHCs may be capable of injecting and dissipating energy from a system in a robust manner, all while producing realistic biological motion.

In this article, we will design a virtual nonholonomic constraint which provably injects energy into the acrobot through human-like giant motion.

#### A. Notation

We use the following notation and terminology in this article. The  $n \times n$  identity matrix is denoted  $I_n$ , and the  $n \times m$  matrix of zeros is denoted  $\mathbf{0}_{n \times m}$ . A matrix  $A \in \mathbb{R}^{n \times m}$  is *right semi-orthogonal* if  $AA^T = I_n$  and is *left semi-orthogonal* if  $A^T A = I_m$ . For  $A \in \mathbb{R}^{n \times m}$  and  $B \in \mathbb{R}^{p \times m}$ , we define  $[A; B] \in \mathbb{R}^{(n+p) \times m}$  as the matrix obtained by stacking  $A$  on top of  $B$ . Given  $\sigma_1, \dots, \sigma_n \in \mathbb{R}$ , we define  $\text{diag}(\sigma_1, \dots, \sigma_n) \in \mathbb{R}^{n \times n}$  as the diagonal matrix whose value at row  $i$ , column  $i$  is  $\sigma_i$ . For  $T > 0$ , the set of real numbers modulo  $T$  is denoted  $[\mathbb{R}]_T$ , with  $[\mathbb{R}]_\infty := \mathbb{R}$ . The gradient of a matrix-valued function  $A : \mathbb{R}^m \rightarrow \mathbb{R}^{n \times n}$  is the block matrix of stacked partial derivatives,  $\nabla_x A := [\frac{\partial A}{\partial x_1}; \dots; \frac{\partial A}{\partial x_m}] \in \mathbb{R}^{nm \times n}$ . Given two matrices  $A \in \mathbb{R}^{n \times m}$  and  $B \in \mathbb{R}^{r \times s}$ , the Kronecker product  $A \otimes B \in \mathbb{R}^{nr \times ms}$  (see [17]) is the matrix

$$A \otimes B = \begin{bmatrix} A_{1,1}B & \cdots & A_{1,m}B \\ \vdots & \ddots & \vdots \\ A_{n,1}B & \cdots & A_{n,m}B \end{bmatrix}. \quad (1)$$

The Poisson bracket [18] between the functions  $f(q, p)$  and  $g(q, p)$  is

$$[f, g] := \sum_{i=1}^n \frac{\partial f}{\partial p_i} \frac{\partial g}{\partial q_i} - \frac{\partial f}{\partial q_i} \frac{\partial g}{\partial p_i}. \quad (2)$$

Finally, the Kronecker delta  $\delta_i^j = 1$  if  $i = j$  and 0 otherwise.

## II. PROBLEM FORMULATION

We will use the simplified acrobot model in Figure 2, where we assume the torso and leg rods are of equal length  $l$  with equal point masses  $m$  at the tips. A real gymnast cannot swing their legs in full circles, though they are usually flexible enough to raise them parallel to the floor; hence, we assume the leg angle  $q_a$  lies in  $[-Q_a, Q_a]$  for some  $Q_a \in [\frac{\pi}{2}, \pi]$ . We also ignore any dissipative forces.

The acrobot has inertia matrix  $M$ , potential function  $V$  (with respect to the horizontal bar), and input matrix  $B$  given as follows:

$$M(q) = \begin{bmatrix} ml^2(3 + 2\cos(q_a)) & ml^2(1 + \cos(q_a)) \\ ml^2(1 + \cos(q_a)) & ml^2 \end{bmatrix}, \quad (3)$$

$$V(q) = -mgl(2\cos(q_u) + \cos(q_u + q_a)), \quad (4)$$

$$B = [0; 1]. \quad (5)$$

For reasons that will become clear in later sections of this article, we will use Hamiltonian mechanics to derive the dynamics of the acrobot. For this we require the conjugate of momenta,  $p = (p_u, p_a) = M(q)\dot{q}$ . The dynamics of the acrobot in  $(q, p)$  coordinates are given in (6). For shorthand, we write  $c_u := \cos(q_u)$ ,  $c_a := \cos(q_a)$ , and  $c_{ua} := \cos(q_u + q_a)$ ; likewise,  $s_u := \sin(q_u)$ ,  $s_a := \sin(q_a)$ , and  $s_{ua} := \sin(q_u + q_a)$ .

$$\begin{aligned} \mathcal{H}(q, p) &= \frac{1}{2}p^\top M^{-1}(q)p - mgl(2c_u + c_{ua}), \\ \begin{cases} \dot{q} &= M^{-1}(q)p, \\ \dot{p}_u &= -mgl(2s_u + s_{ua}), \\ \dot{p}_a &= -\frac{1}{2}p^\top \nabla_{q_a} M^{-1}(q)p - mgl s_{ua} + \tau. \end{cases} \end{aligned} \quad (6)$$

The control input is a force  $\tau \in \mathbb{R}$  affecting only the dynamics of  $p_a$ , representing a torque acting on the hip joint.

Our goal is to design a smooth function  $f : \mathbb{S}^1 \times \mathbb{R}$  such that the relation  $q_a = f(q_u, p_u)$  is a regular VNHC, where the constrained dynamics of the acrobot (under this constraint) gain energy on some set  $D$  in the sense of Definition 1. We will formally define regularity in the next section. Essentially, if the constraint meets some regularity conditions then it can be stabilized via feedback.

*Definition 1:* Let  $\mathcal{Q}$  be an  $n$ -dimensional smooth generalized cylinder. Let  $f : \mathcal{Q} \rightarrow \mathcal{Q} \times \mathbb{R}^n$  be a smooth vector field and let  $D \subset \mathcal{Q}$  be open. The system described by  $\dot{x} = f(x)$  gains energy on  $D$  if, for all compact sets  $K \subset D$  and for almost every initial condition  $x(0) \in K$ , there exists  $T > 0$  such that  $x(t) \notin K$  ( $\forall t > T$ ). The system loses energy on  $D$  if it gains energy in negative-time.

Note that any system satisfying Definition 1 can have unstable equilibria on  $D$ , but not limit cycles nor closed orbits.

Before embarking on our design problem, let us summarize the relevant theory of VNHCs.

### III. THEORY OF VNHCs

#### A. Simply Actuated Hamiltonian Systems

Take a mechanical system modelled with generalized coordinates  $q = (q_1, \dots, q_n)$  on a configuration manifold  $\mathcal{Q} = [\mathbb{R}]_{T_1} \times \dots \times [\mathbb{R}]_{T_n}$ , where  $T_i = 2\pi$  if  $q_i$  is an angle and  $T_i = \infty$  if  $q_i$  is a displacement. The corresponding generalized velocities are  $\dot{q} = (\dot{q}_1, \dots, \dot{q}_n) \in \mathbb{R}^n$ .

Suppose this system has Lagrangian  $\mathcal{L}(q, \dot{q}) = 1/2 \dot{q}^\top D(q)\dot{q} - P(q)$ , where the potential energy  $P : \mathcal{Q} \rightarrow \mathbb{R}$  is smooth, and the inertia matrix  $D : \mathcal{Q} \rightarrow \mathbb{R}^{n \times n}$  is smooth and positive definite for all  $q \in \mathcal{Q}$ . The conjugate of momentum to  $q$  is the vector  $p := \partial \mathcal{L} / \partial \dot{q} = D(q)\dot{q} \in \mathbb{R}^n$ . As per [18], the Hamiltonian of the system in  $(q, p)$  coordinates is

$$\mathcal{H}(q, p) = \frac{1}{2}p^\top D^{-1}(q)p + P(q), \quad (7)$$

with dynamics

$$\begin{cases} \dot{q} &= \nabla_p \mathcal{H}, \\ \dot{p} &= -\nabla_q \mathcal{H} + B(q)\tau, \end{cases} \quad (8)$$

where  $\tau \in \mathbb{R}^k$  is a vector of generalized input forces and the input matrix  $B : \mathcal{Q} \rightarrow \mathbb{R}^{n \times k}$  is full rank for all  $q \in \mathcal{Q}$ . If  $k < n$ , we say the system is *underactuated* with degree of underactuation  $(n - k)$ .

Using the matrix Kronecker product, it is easy to show that (8) expands to

$$\begin{cases} \dot{q} &= D^{-1}(q)p, \\ \dot{p} &= -\frac{1}{2}(I_n \otimes p^\top) \nabla_q D^{-1}(q)p - \nabla_q P(q) + B(q)\tau. \end{cases}$$

Because  $\tau$  is transformed by  $B(q)$ , it is not obvious how any particular input force  $\tau_i$  affects the system. As a first step in addressing this problem, we make the following assumptions.

*Assumption 1:* The input matrix  $B(q) \equiv B \in \mathbb{R}^{n \times k}$  is constant, full rank, and  $k < n$ .

*Assumption 2:* There exists a right semi-orthogonal matrix  $B^\perp \in \mathbb{R}^{(n-k) \times n}$  which is a left-annihilator for  $B$ .

Note that Assumption 2 requires the rows of  $B^\perp$  be unit vectors that are mutually orthogonal. When  $k = (n - 1)$ , Assumption 2 can be removed because it is automatically implied by Assumption 1.

The above assumptions allow us to define a canonical coordinate transformation of (7) which decouples the input forces. To define this transformation we will make use of the following lemma.

**Lemma 2:** Suppose Assumption 1 holds. Then there exists a nonsingular matrix  $\hat{T} \in \mathbb{R}^{k \times k}$  so that the regular feedback transformation

$$\tau = \hat{T}\hat{\tau}$$

has a new input matrix  $\hat{B}$  for  $\hat{\tau}$  which is left semi-orthogonal.

*Proof:* Since  $B$  is constant and full rank, it has a singular value decomposition  $B = U^\top \Sigma V$  where  $\Sigma = [\text{diag}(\sigma_1, \dots, \sigma_k); \mathbf{0}_{(n-k) \times k}]$ ,  $\sigma_i > 0$ , and  $U \in \mathbb{R}^{n \times n}$ ,  $V \in \mathbb{R}^{k \times k}$  are unitary matrices [19]. Defining  $T = \text{diag}(1/\sigma_1, \dots, 1/\sigma_k)$  and assigning the regular feedback transformation  $\tau = VT\hat{\tau}$  yields a new input matrix  $\hat{B} = BVT$  for  $\hat{\tau}$  such that  $\hat{B}^\top \hat{B} = T^\top \Sigma^\top \Sigma T = I_k$ . ■

In light of Lemma 2, there is no loss of generality in assuming that the input matrix is left semi-orthogonal. Now, let  $\mathbf{B} := [B^\perp; B^\top]$ . Since  $B^\perp$  is a left annihilator of  $B$  and both  $B^\perp$  and  $B^\top$  are right semi-orthogonal, one can easily show that  $\mathbf{B}$  is an orthogonal matrix.

**Theorem 3:** Take the Hamiltonian system (7) and suppose Assumptions 1 and 2 hold. The coordinate transformation  $(\tilde{q} = \mathbf{B}q, \tilde{p} = \mathbf{B}p)$  is a canonical transformation and the resulting dynamics are given by

$$\begin{aligned} \mathcal{H}(\tilde{q}, \tilde{p}) &= \frac{1}{2} \tilde{p}^\top M^{-1}(\tilde{q}) \tilde{p} + V(\tilde{q}), \\ \begin{cases} \dot{\tilde{q}} = M^{-1}(\tilde{q}) \tilde{p}, \\ \dot{\tilde{p}} = -\frac{1}{2} (I_n \otimes \tilde{p}^\top) \nabla_{\tilde{q}} M^{-1}(\tilde{q}) \tilde{p} \\ \quad - \nabla_{\tilde{q}} V(\tilde{q}) + \begin{bmatrix} \mathbf{0}_{(n-k) \times k} \\ I_k \end{bmatrix} \tau, \end{cases} \end{aligned} \quad (9)$$

where  $M^{-1}(\tilde{q}) := \mathbf{B}D^{-1}(\mathbf{B}^\top \tilde{q})\mathbf{B}^\top$  and  $V(\tilde{q}) := P(\mathbf{B}^\top \tilde{q})$ .

*Proof:* Since  $\mathbf{B}$  is constant, this transformation satisfies  $\partial \tilde{q}_i / \partial p_j = \partial \tilde{p}_i / \partial q_j = 0$  for all  $i, j \in \{1, \dots, n\}$ . This implies the Poisson brackets  $[\tilde{q}_i, \tilde{q}_j]$  and  $[\tilde{p}_i, \tilde{p}_j]$  are both zero. Then, since  $\mathbf{B}$  is orthogonal,  $[\tilde{p}_i, \tilde{q}_j] = (\mathbf{B}_i)^\top (\mathbf{B}^\top)_j = \delta_i^j$ . By (45.10) in [18], this is a canonical transformation and the new Hamiltonian is  $\mathcal{H}(\mathbf{B}^\top \tilde{q}, \mathbf{B}^\top \tilde{p})$ . Finally, since  $\dot{\tilde{p}} = \mathbf{B}\dot{p}$ , the input matrix for the system in  $(\tilde{q}, \tilde{p})$  coordinates is  $\mathbf{B}B = [\mathbf{0}_{(n-k) \times k}; I_k]$ , which proves the theorem. ■

We call the  $(\tilde{q}, \tilde{p})$  coordinates *simply actuated coordinates*. The first  $(n-k)$  configuration variables in  $\tilde{q}$ , labelled  $q_u$ , are the *unactuated coordinates*; the remaining  $k$  configuration variables, labelled  $q_a$ , are the *actuated coordinates*. The corresponding  $(p_u, p_a)$  in  $\tilde{p}$  are the *unactuated* and *actuated momenta*, respectively.

## B. Virtual Nonholonomic Constraints

Griffin and Grizzle [13] were the first to define relative degree two nonholonomic constraints which can be enforced through state feedback. Horn et. al later extended their results in [14] to derive the constrained dynamics for a certain class of mechanical systems.

These researchers made use of the unactuated conjugate of momentum, but they developed their results in the Lagrangian framework. In particular, they focused on Lagrangian systems with degree of underactuation one. In this section we reformulate their ideas into the Hamiltonian framework and extend the definition of a virtual nonholonomic constraint to systems with higher degree of underactuation. This reformulation will provide us with better intuition and a more explicit form of the constrained dynamics.

For the rest of this section we take the system of inquiry to be a Hamiltonian mechanical system in simply actuated coordinates, as in (9). For simplicity of notation, we relabel  $(\tilde{q}, \tilde{p})$  to  $(q, p)$ .

**Definition 4:** A *virtual nonholonomic constraint (VNHC)* of order  $k$  is a relation  $h(q, p) = 0$  where  $h : \mathcal{Q} \times \mathbb{R}^n \rightarrow \mathbb{R}^k$  is  $C^2$ ,  $\text{rank}([dh_q, dh_p]) = k$  for all  $(q, p) \in h^{-1}(0)$ , and there exists a feedback controller  $\tau(q, p)$  rendering the *constraint manifold*  $\Gamma$  invariant, where

$$\Gamma = \{(q, p) \mid h(q, p) = 0, dh_q \dot{q} + dh_p \dot{p} = 0\}. \quad (10)$$

The constraint manifold is a  $2(n-k)$ -dimensional closed embedded submanifold of  $\mathcal{Q} \times \mathbb{R}^n$ . A VNHC thereby allows us to study a reduced-order model of the system: it reduces the original  $2n$  differential equations to  $2(n-k)$  equations. In particular, if  $k = (n-1)$ , the constraint manifold is *always* 2-dimensional and its dynamics can be plotted on a plane.

We often want to stabilize a constraint within some neighbourhood of  $\Gamma$ . To see when this is possible, let us define the error output  $e = h(q, p)$ . If any component of  $e_i$  has relative degree 1, we may not be able to stabilize  $\Gamma$ : we can always guarantee  $e_i \rightarrow 0$ , but not necessarily  $\dot{e}_i \rightarrow 0$ . It is for this reason that we define the following special type of VNHC.

**Definition 5:** A VNHC  $h(q, p) = 0$  of order  $k$  is *regular* if the output  $e = h(q, p)$  is of relative degree  $\{2, 2, \dots, 2\}$  everywhere on the constraint manifold  $\Gamma$ .

The authors of [13], [14] observed that relations which use only the unactuated conjugate of momentum often have vector relative degree  $\{2, \dots, 2\}$ . Indeed, we shall now provide a characterization of regularity which shows that regular constraints cannot use the actuated momentum at all.

To ease notation in the rest of this section, we use the following shorthand:

$$\mathcal{A}(q, p_u) := dh_q(q, p_u)M^{-1}(q), \quad (11)$$

$$\mathcal{M}(q, p) := (I_{n-k} \otimes p^\top) \nabla_{q_u} M^{-1}(q). \quad (12)$$

*Theorem 6:* A relation  $h(q, p) = 0$  for system (9) is a regular VNHC of order  $k$  if and only if  $dh_{p_a} = \mathbf{0}_{k \times k}$  and

$$\text{rank} \left( (\mathcal{A}(q, p_u) - dh_{p_u} \mathcal{M}(q, p)) \begin{bmatrix} \mathbf{0}_{(n-k) \times k} \\ I_k \end{bmatrix} \right) = k,$$

everywhere on the constraint manifold  $\Gamma$ .

*Proof:* Let  $e = h(q, p) \in \mathbb{R}^k$ . If  $dh_{p_a} \neq \mathbf{0}_{k \times k}$  for some  $(q, p) \in \Gamma$ , then  $\tau$  appears in  $\dot{e}$  and the VNHC is not of relative degree  $\{2, \dots, 2\}$ . Suppose now that  $dh_{p_a} = \mathbf{0}_{k \times k}$ . Then  $\dot{e} = \mathcal{A}(q, p_u)p - dh_{p_u} (1/2 \mathcal{M}(q, p)p + \nabla_{q_u} V(q))$ . Taking one further derivative provides  $\ddot{e} = (\star) - dh_{p_u} (1/2 d/dt (\mathcal{M}(q, p)p)) + \mathcal{A}(q, p_u)[\mathbf{0}_{(n-k) \times k}; I_k]\tau$ , where  $(\star)$  is a continuous function of  $q$  and  $p$ . One can further show that  $dh_{p_u} (1/2 d/dt (\mathcal{M}(q, p)p)) = (\star) + dh_{p_u} \mathcal{M}(q, p)[\mathbf{0}_{(n-k) \times k}; I_k]\tau$ . Hence,

$$\ddot{e} = (\star) + (\mathcal{A}(q, p_u) - dh_{p_u} \mathcal{M}(q, p)) \begin{bmatrix} \mathbf{0}_{(n-k) \times k} \\ I_k \end{bmatrix} \tau,$$

which we write as  $\ddot{e} = E(q, p) + H(q, p)\tau$  for appropriate  $E$  and  $H$ . From the definition of regularity, the VNHC  $h$  is regular when  $e$  is of relative degree  $\{2, \dots, 2\}$ , which is true if and only if the matrix premultiplying  $\tau$  is nonsingular, and hence that  $H$  is invertible. This proves the theorem. ■

Under additional mild conditions (see [20]), a regular VNHC of order  $k$  can be stabilized by the output-linearizing phase-feedback controller

$$\tau(q, p) = -H^{-1}(q, p) (E(q, p) + k_p e + k_d \dot{e}), \quad (13)$$

where  $k_p, k_d > 0$  are control parameters which can be tuned on the resulting error dynamics  $\ddot{e} = -k_p \dot{e} - k_d \ddot{e}$ .

In Section IV we will enforce a regular constraint on the acrobot of the form  $h(q, p) = q_a - f(q_u, p_u)$ , where the actuators track a function of the unactuated variables. Regular constraints of this form always meet the mild conditions from [20], and hence we can stabilize the constraint manifold using (13). Since  $q_a$  is constrained to be a function of the unactuated phase variables, intuition tells us the constrained dynamics should be parameterized by  $(q_u, p_u)$ . Unfortunately,  $\dot{q}_u$  depends on  $p_a$ , and for general systems one cannot solve explicitly for  $p_a$  in terms of  $(q_u, p_u)$  because the  $\dot{p}$  dynamics contain the coupling term  $(I_n \otimes p^\top) \nabla_q M(q)p$ .

We now introduce an assumption which allows us to solve for  $p_a$  as a function of  $(q_u, p_u)$ , which in turn allows us to explicitly solve for the constrained dynamics.

*Assumption 3:* The inertia matrix does not depend on the unactuated coordinates, so that  $\nabla_{q_u} M(q) = \mathbf{0}_{n(n-k) \times n}$ .

*Theorem 7:* Let  $\mathcal{H}$  be a mechanical system in simply actuated coordinates satisfying Assumption 3. Let  $h(q, p_u) = 0$  be a regular VNHC of order  $k$  with constraint manifold  $\Gamma$ . Suppose that on  $\Gamma$  one can solve for  $q_a$  as a function  $q_a = f(q_u, p_u)$ . Then the constrained dynamics are given by

$$\begin{aligned} \dot{q}_u &= [I_{n-k} \quad \mathbf{0}_{(n-k) \times k}] M^{-1}(q)p \\ \dot{p}_u &= -\nabla_{q_u} V(q) \end{aligned} \quad \left| \begin{array}{l} q_a = f(q_u, p_u) \\ p_a = g(q_u, p_u) \end{array} \right. , \quad (14)$$

where

$$g(q, p_u) := \left( \mathcal{A}(q, p_u) \begin{bmatrix} \mathbf{0}_{(n-k) \times k} \\ I_k \end{bmatrix} \right)^{-1} \cdot \left( dh_{p_u} \nabla_{q_u} (V(q) - \mathcal{A}(q, p_u) \begin{bmatrix} I_{n-k} \\ \mathbf{0}_{k \times (n-k)} \end{bmatrix} p_u) \right) \Big|_{q_a=f(q_u, p_u)} \quad (15)$$

*Proof:* Setting  $e = h(q, p_u)$  and using Assumption 3, we find that  $\dot{e} = \mathcal{A}(q, p_u)p - dh_{p_u} \nabla_{q_u} V(q)$ . Notice that  $\mathcal{A}(q, p_u)p = \mathcal{A}(q, p_u)[\mathbf{0}_{(n-k) \times k}; I_k]p_a + \mathcal{A}(q, p_u)[I_{n-k}; \mathbf{0}_{k \times (n-k)}]p_u$ . Since  $h(q, p_u)$  is regular,  $\mathcal{A}(q, p_u)$  is invertible. Taking  $e = \dot{e} = 0$ , solving for  $p_a$ , and setting  $q_a = f(q_u, p_u)$  completes the proof. ■

We conclude this section by formalizing the notion of energy injection/dissipation for VNHCs.

*Definition 8:* A regular VNHC  $h(q, p) = 0$  with constraint manifold  $\Gamma$  *injects (dissipates) energy on*  $D \subset \Gamma$  if the constrained dynamics gain (lose) energy everywhere on  $D$  according to Definition 1, except possibly on a set of measure zero.

**Comparison with existing literature:** Horn et.al. provide the constrained dynamics for VNHCs in [16]. Their assumption **H2** is what we call regularity, and our requirement that one can solve for  $q_a = f(q_u, p_u)$  on  $\Gamma$  implies their assumption **H3** holds true. The only real distinction between this section and their work is that we allow for higher degrees of underactuation, and our constrained dynamics are explicit functions of the Hamiltonian phase coordinates  $(q_u, p_u)$ . In fact, our constrained dynamics (14) coincide with their system (17) when one chooses the special case  $\theta_1 = q_u$  and  $\theta_2 = p_u$ . This explicit representation will be beneficial when we apply the theory of VNHCs to the acrobot.

#### IV. THE ACROBOT VNHC

Our goal in this article is to design a VNHC which injects energy into the acrobot through giant-like motion. Recall that the acrobot in Figure 2 has dynamics given by (6), which are repeated here:

$$\begin{aligned} \mathcal{H}(q, p) &= \frac{1}{2} p^\top M^{-1}(q) p - mgl(2c_u + c_{ua}), \\ \begin{cases} \dot{q} &= M^{-1}(q) p, \\ \dot{p}_u &= -mgl(2s_u + s_{ua}), \\ \dot{p}_a &= -\frac{1}{2} p^\top \nabla_{q_a} M^{-1}(q) p - mgl s_{ua} + \tau. \end{cases} \end{aligned}$$

Since the control input  $\tau$  only affects the actuated momentum,  $(q, p)$  are simply actuated coordinates in the phase space  $\mathcal{Q} \times \mathcal{P}$  where  $\mathcal{Q} = \mathbb{S}^1 \times \mathbb{S}^1$ , and  $\mathcal{P} = \mathbb{R} \times \mathbb{R}$ . We can therefore apply the theory from Section III to design a VNHC of the form  $q_a = f(q_u, p_u)$ . Since we need the VNHC to be regular, the following proposition will be useful.

*Proposition 9:* A relation  $h(q, p) = q_a - f(p_u) = 0$  with  $f \in C^2(\mathbb{R}; \mathbb{S}^1)$  is a regular VNHC of order 1 for the acrobot.

*Proof:* The regularity matrix for the acrobot evaluates to  $((1 + c_a)\partial_{q_u} f(q_u, p_u) + (3 + 2c_a))/(ml^2(2 - c_a^2))$ . Since  $\partial_{q_u} f = 0$ , this matrix is strictly positive for all values of  $q_a$ , and hence is full rank everywhere on the constraint manifold. ■

To design our VNHC, we begin by examining a person on a seated swing. The person extends their legs when the swing moves forwards, and retracts their legs when the swing moves backwards. As the swing gains speed, the person leans their body while extending their legs higher, thereby shortening the distance from their center of mass to the pivot and adding more energy to the swing [21].

Now imagine the person's torso is affixed to the swing's rope so they are always upright. Imagine further that the swing has no seat at all, allowing the person to extend their legs beneath them. This position is identical to that of a gymnast on a bar.

The acrobot's legs are rigid rods which cannot retract, so we emulate the person on a swing by pivoting the legs toward the direction of motion. Since a person lifts their legs higher at faster speeds, the acrobot's legs should pivot to an angle proportional to the swing's speed. Because the direction of motion is entirely determined by  $p_u$ , one VNHC which emulates this process is  $q_a = \bar{q}_a \arctan(I p_u)$ , displayed in Figure 3. Here,  $\bar{q}_a \in ]0, 2Q_a/\pi]$  is constant and  $I \in \mathbb{R}$  is a fixed control parameter.

This constraint does not perfectly recreate giant motion, during which the gymnast's legs are almost completely extended [1]. It instead pivots the legs partially during rotations. However, the behaviour is similar enough that this constraint will still inject energy into the acrobot. Our final VNHC is

$$h(q, p) = q_a - \bar{q}_a \arctan(I p_u). \quad (16)$$

Recall that  $(q_u, p_u)$  denote the angle and momentum of the acrobot's torso. By Theorem 7, the constrained acrobot is parameterized fully by  $(q_u, p_u) \in \mathbb{S}^1 \times \mathbb{R}$ . It is easy to show that the constrained dynamics are just the torso dynamics obtained when one swings the legs according to (16). That is, the constrained dynamics are

$$\begin{cases} \dot{q}_u &= \frac{(1 + I^2 p_u^2) p_u + m^2 g l^3 \bar{q}_a I (2s_u + s_{ua})(1 + c_a)}{m l^2 (1 + I^2 p_u^2) (3 + 2c_a)}, \\ \dot{p}_u &= -mgl(2s_u + s_{ua}), \end{cases} \quad (17)$$

subject to  $q_a = \bar{q}_a \arctan(I p_u)$ .

Suppose for a moment that  $I = 0$ , i.e. that the legs stay fully extended. The acrobot becomes a nominal pendulum with two masses, whose total mechanical energy is

$$E(q_u, p_u) := \frac{p_u^2}{10ml^2} + 3mgl(1 - \cos(q_u)). \quad (18)$$

The upright equilibrium of this pendulum is located at  $(q_u, p_u) = (\pi, 0)$ . Imagine the pendulum hits the bottom of the swing arc with momentum  $p_u \neq 0$ . To reach the upright equilibrium, this momentum must be  $p_u = \pm \sqrt{60m^2 g l^3}$  because  $E(\pi, 0) = E(0, \pm \sqrt{60m^2 g l^3})$ . If the momentum is smaller in magnitude, the acrobot will oscillate; if it is larger, the pendulum will rotate around the bar.

When the pendulum is oscillating, its phase  $(q_u, p_u)$  lies in the set

$$\mathcal{O}_1 := \{(q_u, p_u) \in \mathbb{S}^1 \times \mathbb{R} \mid E(q_u, p_u) < E(\pi, 0)\}, \quad (19)$$

which is shown in Figure 4a. If for some  $I \neq 0$  our VNHC injects energy into the acrobot on  $\mathcal{O}_1$ , and the constrained dynamics escape  $\mathcal{O}_1$  in finite time, then the acrobot is guaranteed to perform giant-like motion and begin rotating around the bar.

When the pendulum is rotating with bounded momentum  $|p_u| < \bar{\rho}$  (for some chosen  $\bar{\rho}$ ), the phase must lie inside the rotation domain

$$\mathcal{R}(\rho) := \{(q_u, p_u) \in \mathbb{S}^1 \times \mathbb{R} \mid E(\pi, 0) < E(q_u, p_u) < E(0, \rho)\}. \quad (20)$$



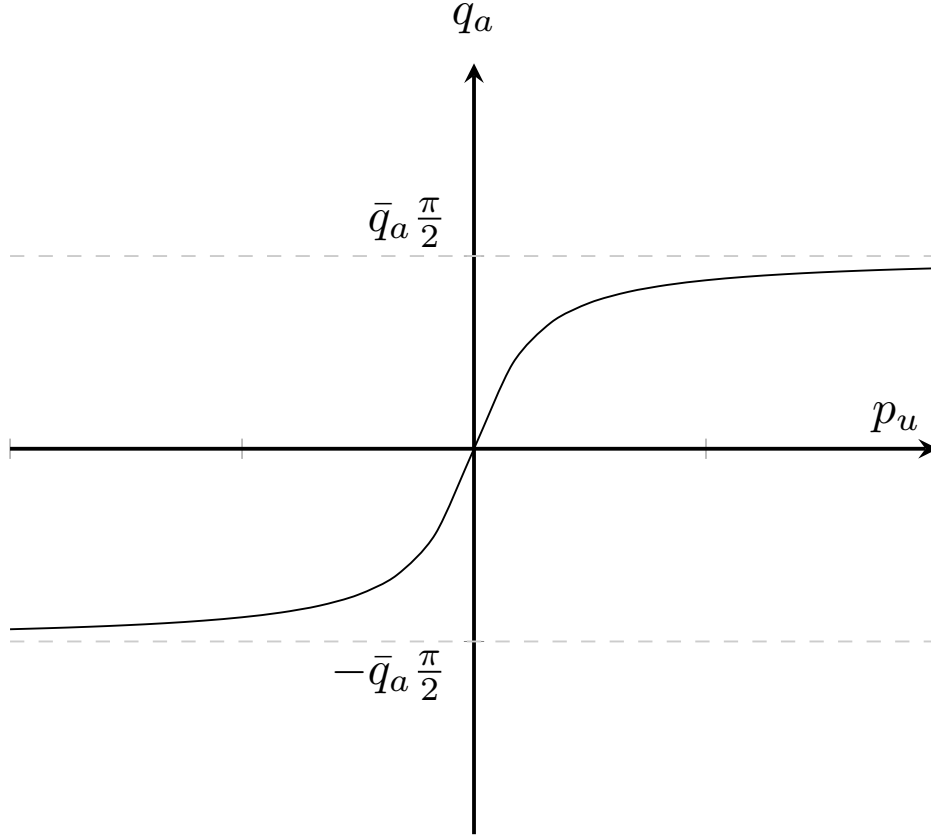


Fig. 3: The acrobot constraint  $q_a = \bar{q}_a \arctan(I p_u)$ .

Connecting the regions (19) and (20) yields the set

$$\mathcal{O}_2(\bar{\rho}) := \{(q_u, p_u) \in \mathbb{S}^1 \times \mathbb{R} \mid E(q_u, p_u) < E(0, \bar{\rho})\}, \quad (21)$$

shown in Figure 4b. If the VNHC injects energy on  $\mathcal{O}_2(\bar{\rho})$  for some  $I \neq 0$ , then the acrobot must necessarily swing up, begin rotating, and eventually rotate with a momentum of at least  $\bar{\rho}$ .

Unfortunately, our VNHC does not always inject energy on  $\mathcal{O}_1$  and  $\mathcal{O}_2(\bar{\rho})$ . If  $I$  is too large, the leg controller saturates and the body oscillates without gaining energy. Choosing  $I$  small enough guarantees the legs will synchronize properly with the body, and the acrobot will begin rotating around the bar. The following theorem provides conditions under which such an  $I$  exists.

*Theorem 10:* Consider the acrobot with Hamiltonian dynamics as in (6).

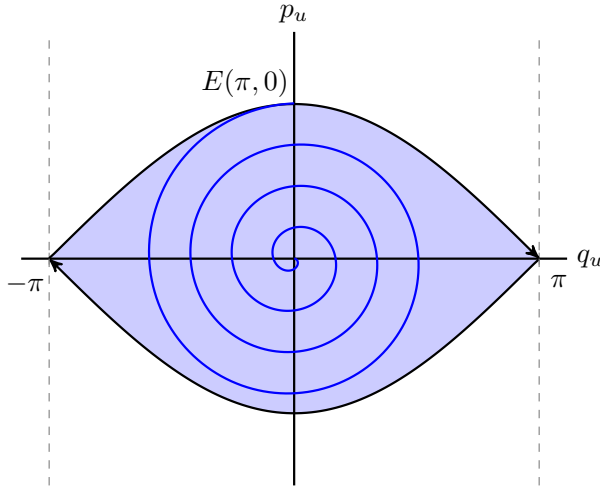
- 1) For any  $m, g, l, \bar{q}_a$ , there exists  $I^* > 0$  such that, for all  $I \in ]0, I^*]$ , the VNHC (16) injects energy into the acrobot on  $\mathcal{O}_1$ . Moreover, almost every orbit will escape the closure of  $\mathcal{O}_1$  in finite time. If instead  $I \in [-I^*, 0[$ , the VNHC dissipates energy.
- 2) Let  $C = m^2 g l^3 \bar{q}_a$  and define  $b : \mathbb{S}^1 \times \mathbb{R}_{>0} \rightarrow \mathbb{R}$  by

$$b(\beta, \rho_0) := \frac{5C \left( \frac{C}{\bar{q}_a} \left( 18s_\beta^2 + 30c_\beta(1 - c_\beta) \right) - c_\beta \rho_0^2 \right)}{|\rho_0| \sqrt{\rho_0^2 - 30m^2 g l^3 (1 - c_\beta)}}.$$

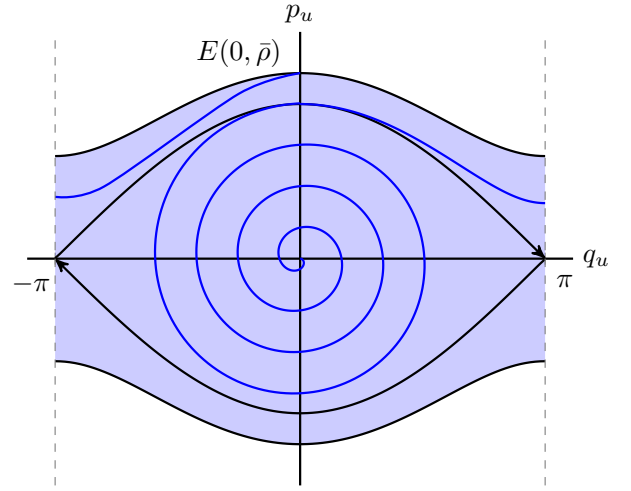
Define  $S(\rho_0) := \int_0^{2\pi} b(\sigma, \rho_0) d\sigma$ . Fix  $\bar{\rho} > \sqrt{60m^2 g l^3}$  and suppose there exists  $\epsilon > 0$  so that  $S(\rho_0) \geq \epsilon$  for all  $\rho_0 \in [\sqrt{60m^2 g l^3}, \bar{\rho}]$ . Then there exists  $I^{**} \in ]0, I^*]$  such that, for all  $I \in ]0, I^{**}]$ , the VNHC (16) injects energy into the acrobot on  $\mathcal{O}_2(\bar{\rho})$ . If instead  $I \in [-I^{**}, 0[$ , the VNHC dissipates energy.

*Proof:* See Section VII. ■

Notice that  $\mathcal{O}_1 \subset \mathcal{O}_2(\bar{\rho})$ , yet Theorem 10 considers these sets separately. This separation is advantageous because the first result holds for any  $m, g, l$ , and  $\bar{q}_a$ . In other words, the first result of Theorem 10 states that all acrobots constrained by (16) will gain enough energy to begin rotating around the bar.



(a) The set  $\mathcal{O}_1$ . An orbit starting in this set (blue) will pass through the level set  $E(\pi, 0)$  of the nominal pendulum.



(b) The set  $\mathcal{O}_2(\bar{\rho})$ . Orbits starting in this set are guaranteed to reach the level set  $E(0, \bar{\rho})$  of the nominal pendulum.

Fig. 4: The sets on which the acrobot gains energy, according to Theorem 10.

For the acrobot to achieve giants with energy  $E(0, \bar{\rho})$ , it must satisfy the assumption on the integral of  $b(\beta, \rho_0)$ . The value of this integral depends on the acrobot's physical parameters. If the assumption holds, there is some control value  $I$  (which depends on  $\bar{\rho}$ ) for which the acrobot will achieve rotations with a momentum of at least  $\bar{\rho}$ .

One can apply the results of Theorem 10 towards energy regulation. For example, one might employ a supervisor which switches between injection and dissipation VNHCs to stabilize a desired energy level  $E_{\text{des}}$ , with some hysteresis to avoid infinite switching. We will explore this idea in Section V.

## V. SIMULATION RESULTS

In Section VI we will test our VNHC on the physical acrobot built by Xingbo Wang [4]. This physical acrobot cannot be modelled by the simplified setup in Figure 2, because the torso and leg links have distributed mass. We must therefore use the more general acrobot model in Figure 5 to represent this system. Let us define

$$\begin{aligned} m_{11}(q) &:= m_a l_u^2 + 2m_a l_u l_{c_a} \cos(q_a) + m_a l_{c_a}^2 + m_u l_{c_u}^2 \\ &\quad + J_u + J_a, \\ m_{12}(q) &:= m_a l_{c_a}^2 + m_a l_u l_{c_a} \cos(q_a) + J_a, \\ m_{22}(q) &:= m_a l_{c_a}^2 + J_a, \end{aligned}$$

where  $J_u$  and  $J_a$  are the moments of inertia of the torso and leg links respectively. The general acrobot has inertia matrix

$$M(q) = \begin{bmatrix} m_{11}(q) & m_{12}(q) \\ m_{12}(q) & m_{22}(q) \end{bmatrix},$$

and potential function

$$V(q) = g(m_a l_{c_a}(1 - c_{ua}) + (m_a l_u + m_u l_{c_u})(1 - c_u)).$$

The dynamic parameters of Wang's acrobot can be found in Table I. Evaluating the mechanical energy of an acrobot with these parameters at the VNHC  $q_a = 0$  yields the mechanical energy of the nominal pendulum,

$$E(q_u, p_u) \approx 396.5501 p_u^2 + 0.5997(1 - \cos(q_u)).$$

We will now simulate the effects of constraining Wang's acrobot with (16), thereby demonstrating that VNHCs are robust to model mismatch. According to Theorem 10, the control parameter  $I$  must be "small" for our VNHC to inject (or dissipate) energy into the simplified acrobot. Unfortunately, the Theorem does not specify how small  $|I|$  must be; while we could make it arbitrarily small in simulations, we will eventually implement this VNHC on a physical testbed where  $|I|$  must be large enough to overcome friction.

Setting  $\bar{q}_a = 1$ , we experimentally determined that  $|I| = 10$  is a viable control parameter, so this is the value we will use for all simulations and experiments. In other words, our injection VNHC is (16) with  $I = 10$  while our dissipation VNHC is (16) with  $I = -10$ .



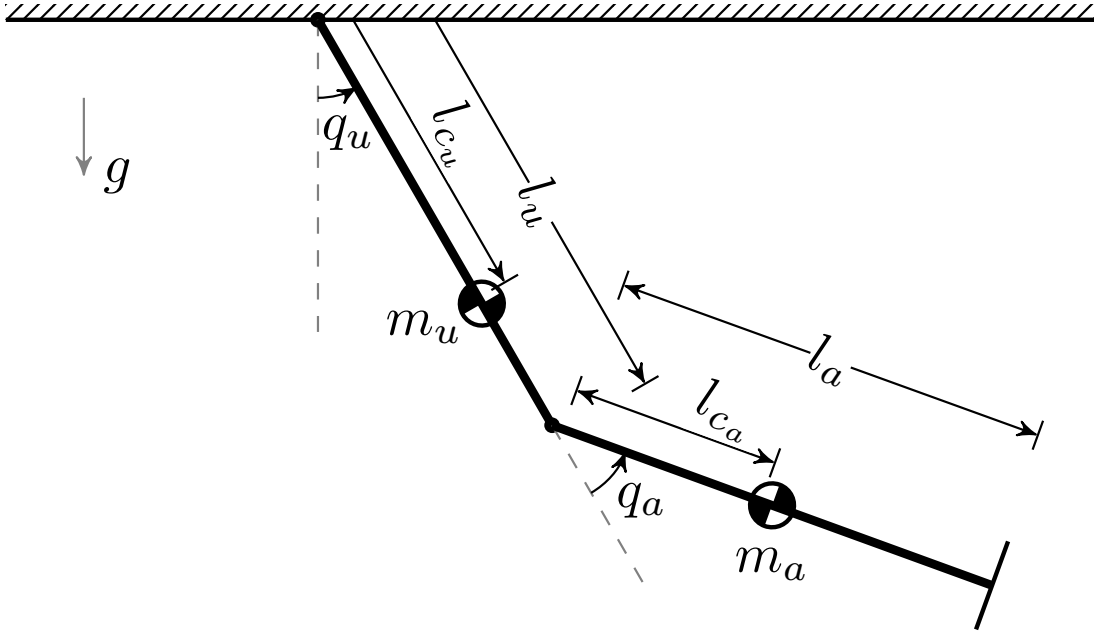


Fig. 5: The general acrobot model, represented by two weighted rods differing in both length and mass.

TABLE I: Physical parameters for the real acrobot.

$m_u$	$m_a$	$l_u$	$l_a$	$l_{cu}$	$l_{ca}$	$J_u$	$J_a$	$g$
0.2112	0.1979	0.148	0.145	0.073	0.083	0.00129	0.00075	9.81

#### A. Energy Injection

We simulated the acrobot constrained by our injection VNHC with initial condition  $(q_u, p_u) = (\pi/32, 0)$  for 30 seconds, and plotted the resulting orbit in Figure 6.

The level set  $E_\pi$  with energy  $E(\pi, 0)$  is outlined in black. Despite the change in acrobot model, this level set remains the boundary between oscillations and rotations for the nominal pendulum. The points where the orbit exits  $E_\pi$  are marked with black stars, with the final departure marked by a red star. Interestingly, our choice of  $I$  is large enough that we observe significant differences between the nominal pendulum and the constrained dynamics:  $E_\pi$  intersects the  $p_u$ -axis at  $|p_u| \approx 0.18$ , yet the constrained acrobot begins rotating once it hits the  $p_u$ -axis at  $|p_u| \approx 0.16$ . This indicates that higher values of  $I$  enable the acrobot to gain energy faster and begin rotating sooner, so long as the actuator does not saturate.

To verify numerically that the acrobot would consistently achieve rotations, we ran a Monte-Carlo [22] simulation where we initialized the acrobot randomly inside the sublevel set

$$\left\{ (q_u, p_u) \in \mathbb{S}^1 \times \mathbb{R} \mid E(q_u, p_u) \leq E\left(\frac{\pi}{32}, 0\right) \right\},$$

and measured how long it took to begin rotating. The results in Figure 7 show that the acrobot always rotated within 20–40 seconds.

#### B. Energy Dissipation

We initialized our acrobot with a rotation at  $(q_u, p_u) = (0, 0.18)$  and simulated the constrained dynamics (under the dissipation VNHC) for 30 seconds. The resulting orbit is plotted in Figure 8. As expected, the acrobot slows down over time. We highlight the locations where the orbit crossed the set  $E_\pi$  by black stars, with the final crossing in red. After this final crossing, the acrobot ceased rotating and its oscillations decayed to zero.

#### C. Oscillation Regulation

Once can use a supervisor to stabilize oscillations by appropriately toggling between injection and dissipation VNHCs. Specifically, one chooses a desired oscillation angle  $q_{des} \in ]0, \pi[$  and, to avoid infinite switching, a hysteresis value  $\delta \in [0, 1]$ . Each time the orbit crosses the  $q_u$ -axis (i.e. when  $p_u = 0$ ) or when  $|q_u| = \pi$ , the supervisor does the following:

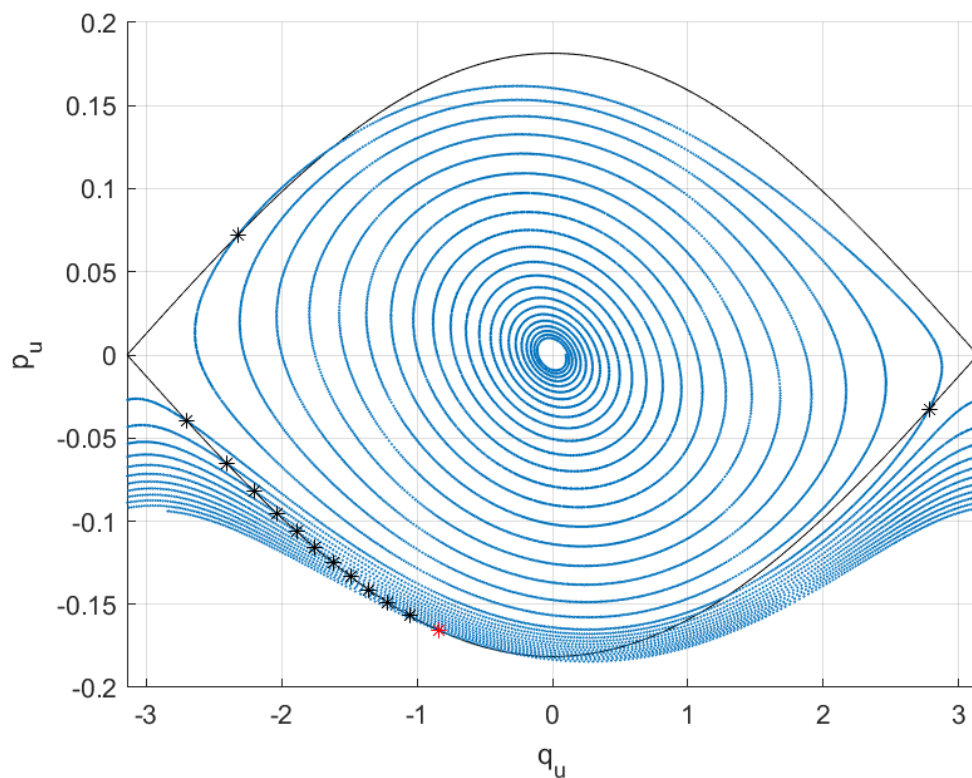


Fig. 6: A simulation of the acrobot gaining energy.

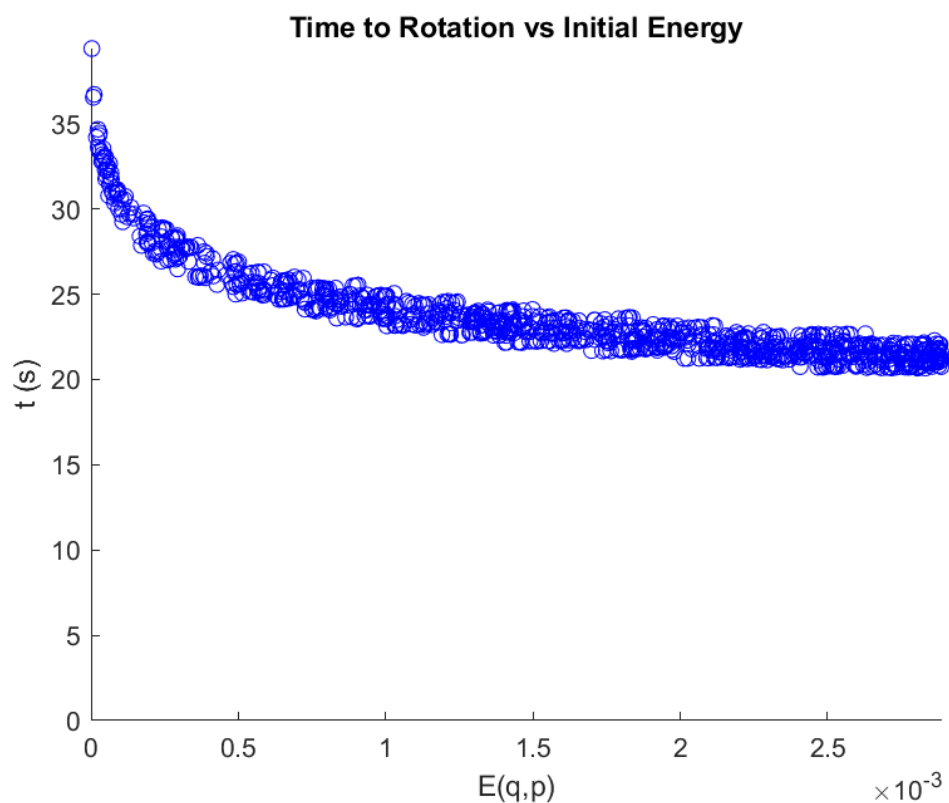


Fig. 7: Monte Carlo simulation for energy injection.

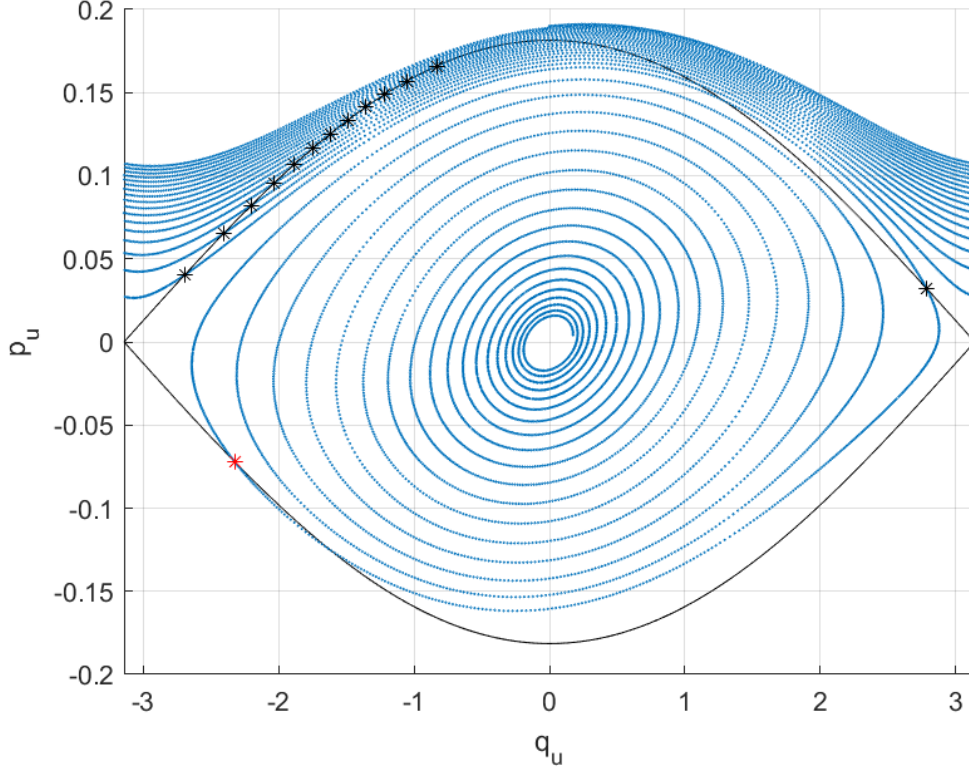


Fig. 8: A simulation of the acrobot dissipating energy.

- If  $|q_u| < (1 - \delta)q_{\text{des}}$ , enable the injection VNHC.
- If  $|q_u| > (1 + \delta)q_{\text{des}}$ , enable the dissipation VNHC.
- If  $(1 - \delta)q_{\text{des}} \leq |q_u| \leq (1 + \delta)q_{\text{des}}$ , keep the leg extended at  $q_a = 0$ . This can be done continuously since  $q_a = 0$  when  $p_u = 0$ .

Figure 9 shows the supervisor stabilizing an oscillation with body angle  $q_{\text{des}} = \pi/2$  and a 5% hysteresis, meaning  $\delta = 0.05$ . The supervisor reevaluated its choice of VNHC at each black star; the red contour corresponds to the part of the orbit where the supervisor kept the leg extended, because the oscillation was within tolerance of  $q_{\text{des}}$ . The solid black line is the desired oscillation, and the dashed black lines show the hysteresis around that orbit.

In Figure 9a the acrobot was initialized at  $(q_u, p_u) = (\pi/32, 0)$ ; here the supervisor injected energy for most of the orbit. In Figure 9b the acrobot was initialized at the rotation  $(q_u, p_u) = (0, 0.19)$ ; here the supervisor dissipated energy. In both cases, the supervisor stabilized the desired oscillation.

#### D. Rotation Regulation

One can also use a supervisor to stabilize rotations. In this case, one chooses a desired rotation rate  $p_{\text{des}} > 0$  and a hysteresis value  $\delta \in [0, 1]$ . Each time the orbit crosses the  $p_u$ -axis (i.e. when  $q_u = 0$ ), the supervisor changes which VNHC is enforced as follows:

- If  $|p_u| < (1 - \delta)p_{\text{des}}$ , enable the injection VNHC.
- If  $|p_u| > (1 + \delta)p_{\text{des}}$ , enable the dissipation VNHC.
- If  $(1 - \delta)p_{\text{des}} \leq |p_u| \leq (1 + \delta)p_{\text{des}}$ , extend the leg fully by setting  $q_a = 0$ . For these simulations, we assume this can be done instantaneously.

Rotation regulation is demonstrated in Figure 10, where the supervisor stabilizes  $p_{\text{des}} = 0.19$  with a 2% hysteresis  $\delta = 0.02$ . The supervisor changed its choice of VNHC at each black star until it was within range of  $p_{\text{des}}$ , at which point it extended the leg (shown in red).

In Figure 10a the acrobot was initialized at  $(q_u, p_u) = (\pi/2, 0)$ ; here the supervisor injected energy until the orbit hit the  $p_u$ -axis near  $p_{\text{des}}$ . In Figure 10b the acrobot was initialized at the faster rotation  $(q_u, p_u) = (0, 0.23)$ ; here the supervisor dissipated energy. In both cases, the desired rotation was stabilized correctly.

Note the difference in shape between the blue rotations of the dissipation VNHC and the red rotation of the nominal pendulum: the red one slows down much more near  $|q_u| = \pi$ . This difference arises because of the size of  $I$ : if  $|I|$  were

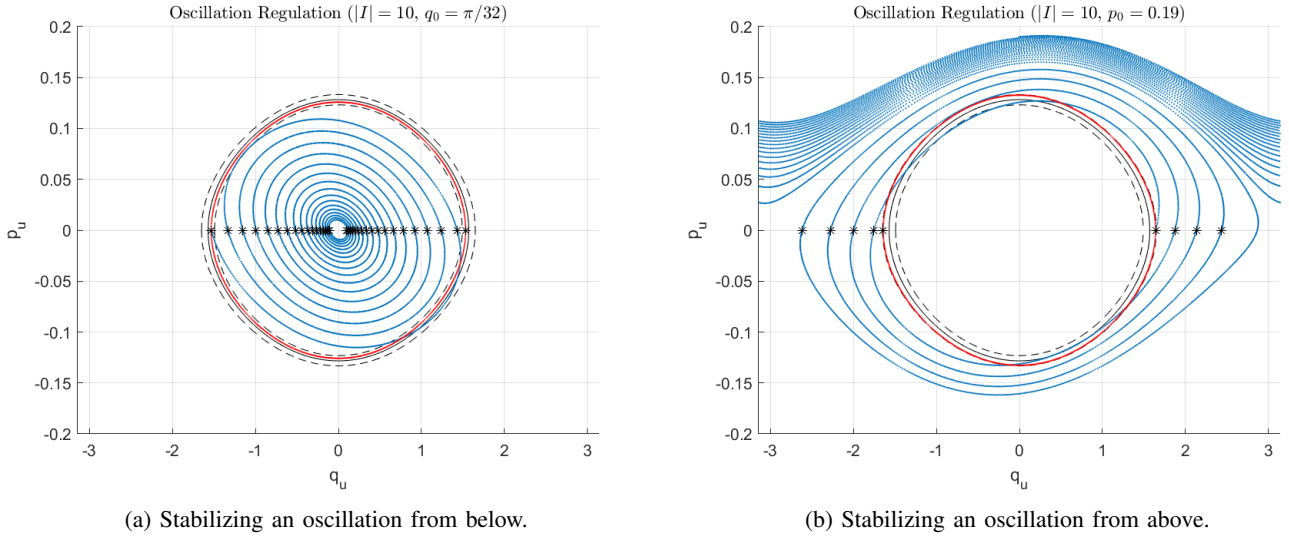


Fig. 9: Using a supervisor to stabilize the oscillation with peak angle  $q_{\text{des}} = \pi/2$ .

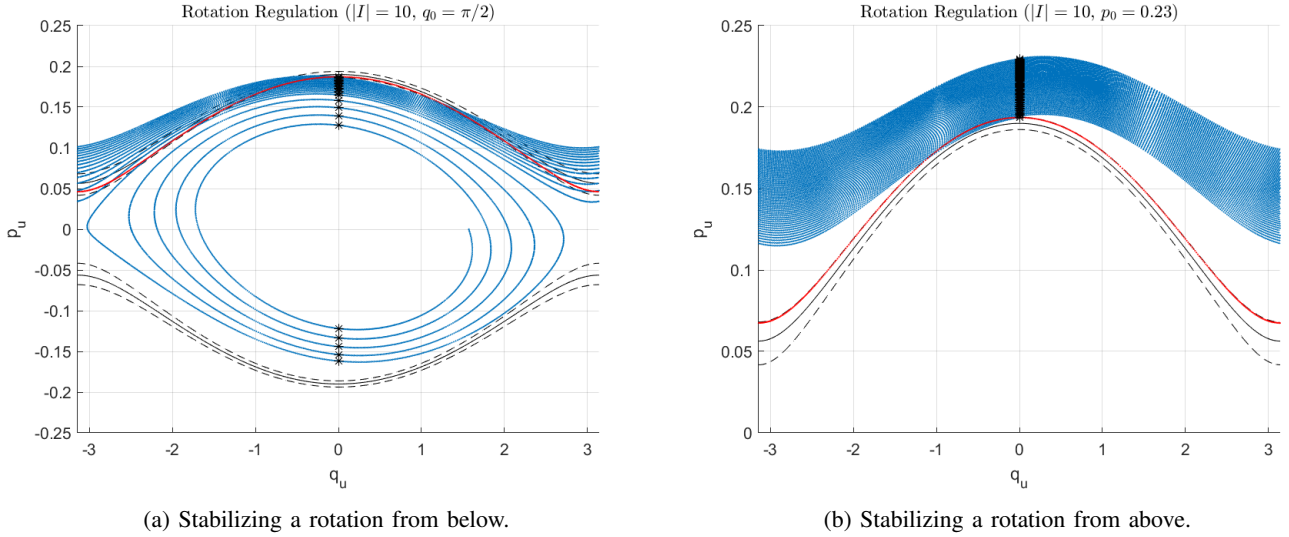


Fig. 10: Using a supervisor to stabilize the rotation with maximal momentum  $p_{\text{des}} = 0.23$ .

smaller, the blue rotations would be more similar in shape to the red one because the constrained dynamics for the dissipation VNHC would be well approximated by the nominal pendulum.

### E. Summary of Results

The simulation results in this section demonstrate the energy regulation capabilities of our VNHC. We were able to stabilize both oscillations and rotations by implementing a control supervisor which toggled between injection, dissipation, and leg-extension VNHCs. In particular, these simulations indicate that our VNHC works even for acrobats whose limbs have differing masses and lengths.

## VI. PHYSICAL EXPERIMENTS

### A. Hardware Description

In this section we will demonstrate that our VNHC is robust to friction, sensor noise, and other real-world considerations by testing it on the physical acrobat built by Xingbo Wang [4] (Figure 11). This platform was given the name SUGAR, which stands for Simple Underactuated Gymnastics and Acrobatics Robot. Its dynamic parameters are outlined in Table I.

SUGAR is comprised of two 3D-printed links: a torso and a leg. The torso link houses an Arduino Nano microcontroller unit (MCU) which controls a Dynamixel RX24F servo motor between the torso and the leg. The MCU and the motor are powered by a 12V battery held in a compartment in the leg.

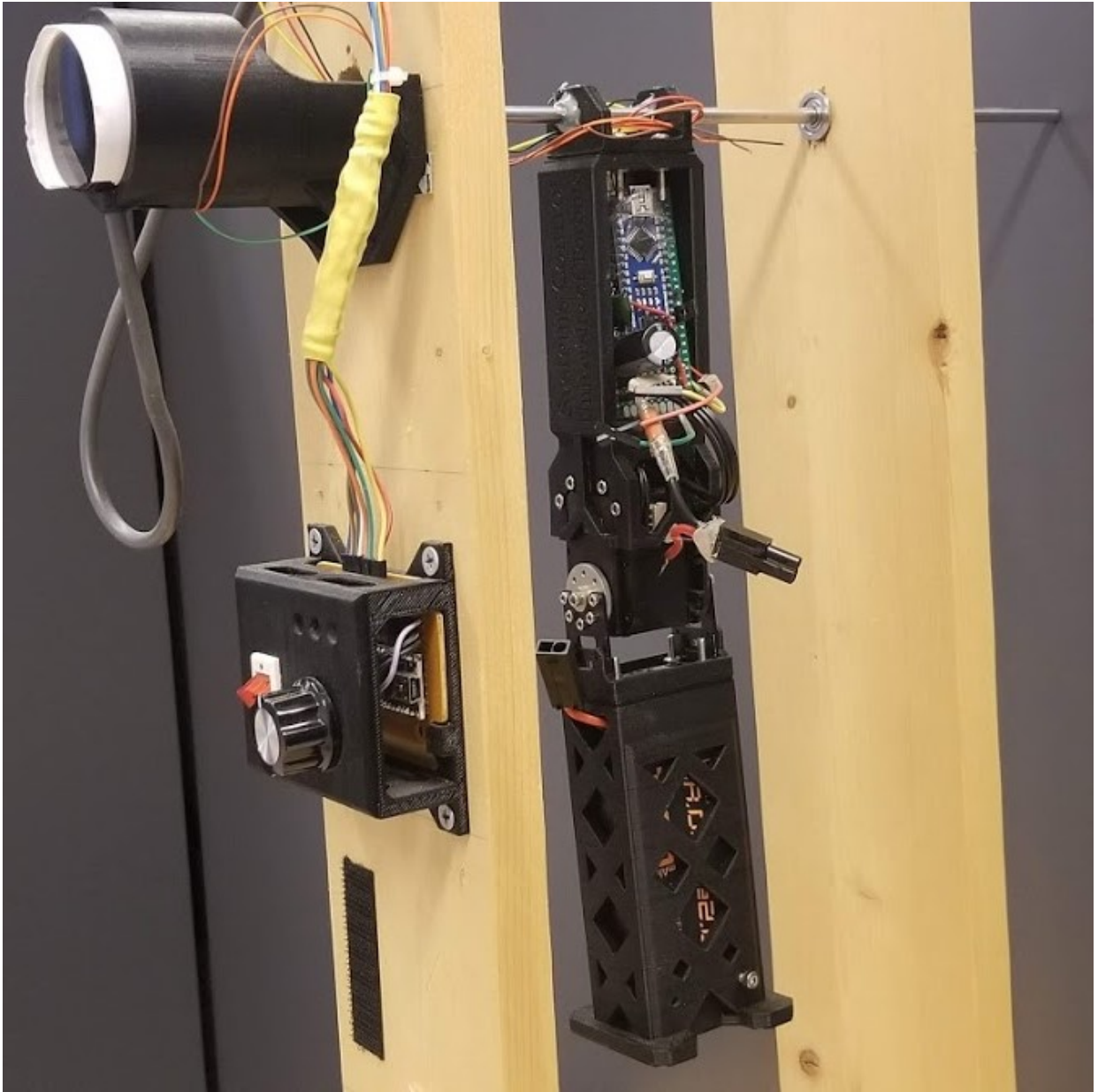


Fig. 11: SUGAR is the physical acrobot built by Wang [4].

The torso is rigidly attached to a metal bar, which is held up by two wooden posts. On the exterior of one post is a control box with a power switch and a second Arduino Nano 328. The purpose of this control box is to read measurements from a rotary encoder connected to the metal bar, and to transmit these measurements to the MCU. The two Arduinos communicate through wires attached to a slip ring on the metal bar, and the signals are transmitted via I2C. The control box also provides a USB interface which allows the user to read the data from the acrobot in real time.

The rotary encoder directly measures  $q_u$ , and the Dynamixel servo motor provides measurements of  $q_a$ . However, there are no sensors measuring the velocity  $\dot{q}$ , which means we cannot directly evaluate  $p_u$  and  $p_a$ . To resolve this issue, the MCU estimates  $\dot{q}$  by applying a washout filter to sequential measurements of  $q$ . We then compute  $p = M(q)\dot{q}$  for use in the VNHC controller.

Communication between the Arduinos restricts the sampling rate of  $p$  to 500Hz. This low sampling rate results in a noisy momentum signal which suffers from noticeable phase lag. This also rate-limits the control signal to 500Hz, which impacts any control implementation.

Finally, The Dynamixel servo motor does not have a torque control mode; instead, we can assign the servo setpoint at iteration  $k \in \mathbb{Z}_{>0}$  via  $q_a^k = \arctan(Ip_u^{k-1})$ . Unfortunately, this negatively affects the stabilization to the constraint manifold because we are introducing timing errors from the servo's built-in PID controller.



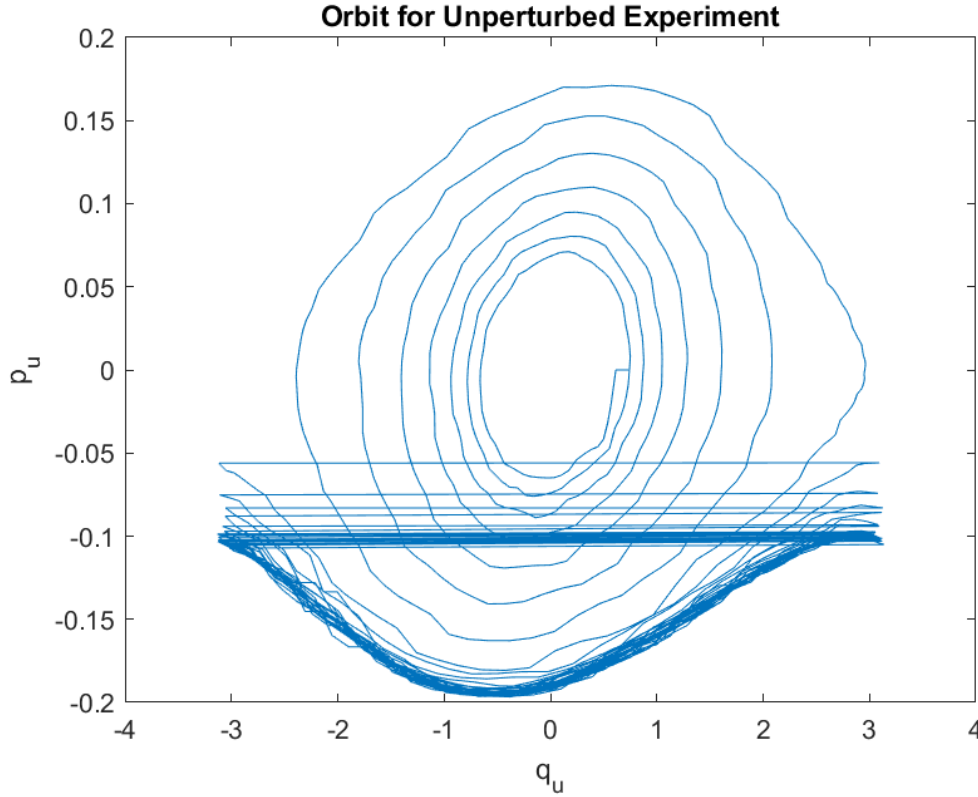


Fig. 12: SUGAR's orbit during the baseline energy injection test.

### B. Experimental Results

We performed the following tests on SUGAR with the energy injection VNHC.

- 1) **Baseline Test:** we initialized the acrobot at  $(q_u, p_u) \approx (\pi/8, 0)$ . The resulting orbit in Figure 12 shows that SUGAR clearly gaining energy over time. Its motion looks similar to that of the energy injection simulation (Figure 6), though its energy gain ceases once it reaches a rotation with energy  $E(0, 0.195)$ .
- 2) **Stop Test:** we initialized SUGAR at  $(q_u, p_u) \approx (\pi, 0)$ , let it run for 15 seconds, then stopped it at the bottom of its arc. The resulting orbit is shown in Figure 13. The blue rotation curve corresponds to the orbit before the disturbance, while the red spiral confirms that the acrobot begins oscillating after it is stopped. Despite the disturbance, it gains energy and eventually starts rotating again.
- 3) **Push Test:** to see how SUGAR responds when pushed, we allowed it to rotate undisturbed for 15 seconds and then pushed it in its direction of motion. The orbit in Figure 14a shows that the acrobot, when pushed, rotates with energy  $E(0, -0.22)$ , but then slows down until it reaches a rotation with energy  $E(0, -0.195)$ . We repeated this test by pushing SUGAR against its direction of motion. The orbit in Figure 14b demonstrates that the acrobot readily changes direction, and quickly achieves its maximum speed with energy  $E(0, 0.195)$ .

In simulation, the acrobot was able to gain energy even when initialized with energy  $E(q_u, p_u) > E(0, 0.195)$ . The baseline and push tests suggest that our VNHC injects energy into SUGAR only on  $\mathcal{O}_2(0.195)$ . This difference between simulation and implementation is likely due to friction.

We had hoped to show experimental results for dissipation and oscillation/rotation regulation. Unfortunately the Dynamixel RX24F servo motor broke before we could perform these experiments. These motors are no longer in production at the time of writing this article, so SUGAR has been retired from service.

### C. Summary of Results

We performed three tests on SUGAR: a baseline energy injection test, a stop test, and a push test. These experiments demonstrate that VNHC-based energy injection is robust to significant model mismatch, friction, sensor noise, discretized control implementation, rate-limited measurement and control signals, and dramatic external disturbances.

## VII. PROOF OF THEOREM 10

**TODO: prove Thm 10**



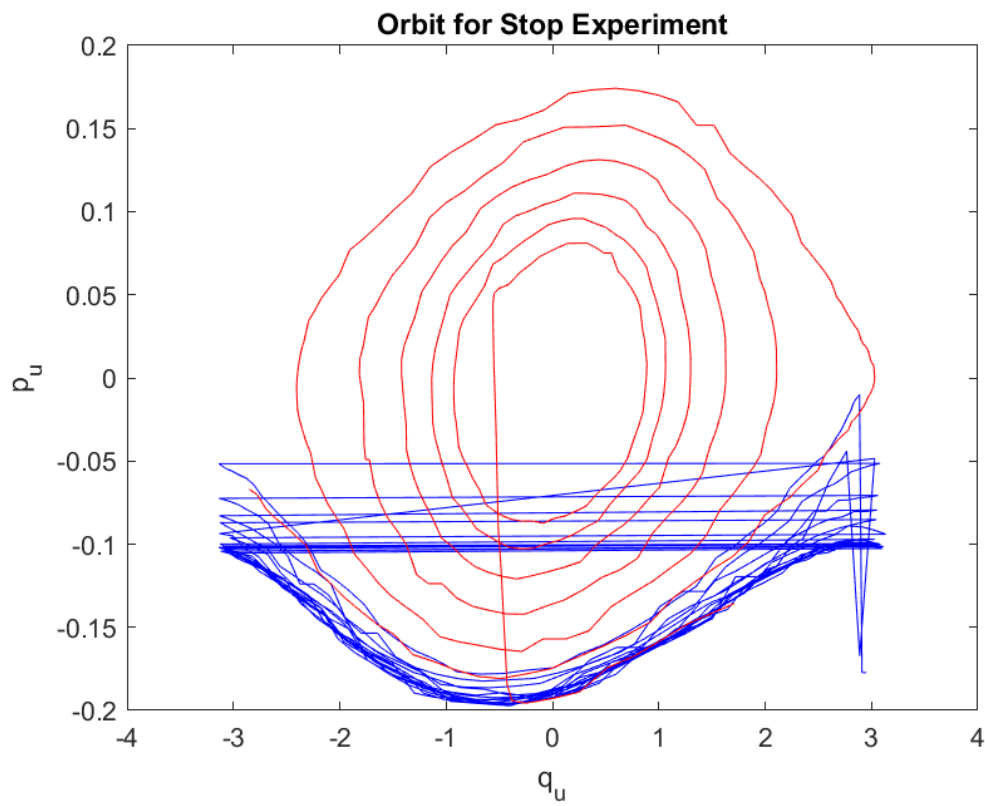
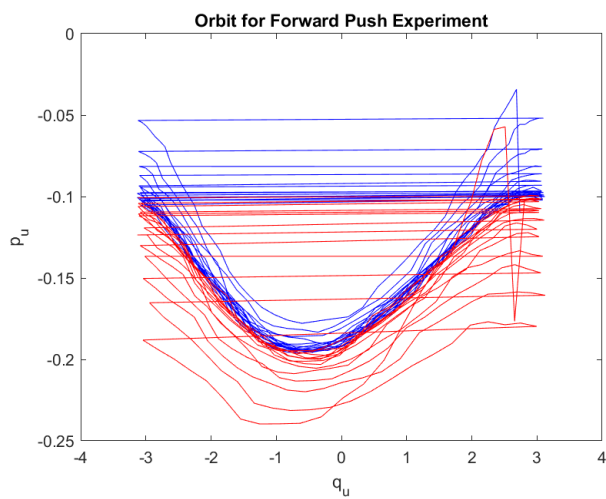
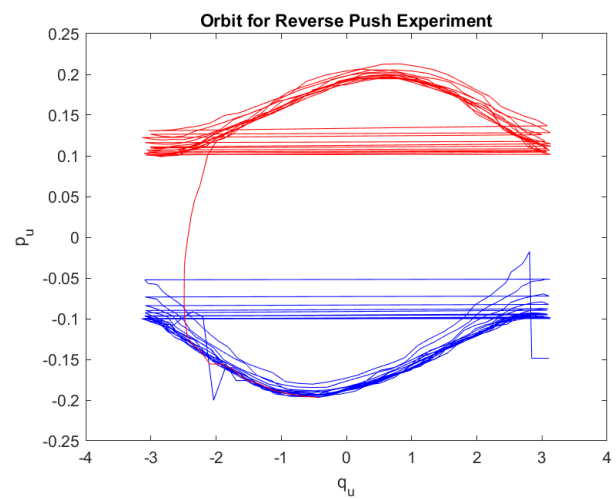


Fig. 13: SUGAR's orbit before (blue) and after (red) stopping.



(a) The forwards push test.



(b) The reverse push test.

Fig. 14: SUGAR's orbit before (blue) and after (red) pushing.

## VIII. CONCLUSION

In this article we redeveloped the framework of virtual nonholonomic constraints for underactuated mechanical systems with arbitrary degree of underactuation. We applied this framework towards the acrobot, and designed a constraint which emulates giant motion from gymnastics. We proved this constraint will inject energy into the simplified acrobot whose limbs are massless rods of equal length, with equal masses at the tips. We then performed simulations and physical experiments of this VNHC. These demonstrated that virtual nonholonomic constraints are capable of injecting and dissipating energy in a robust manner, all while producing realistic biological motion.

## REFERENCES

- [1] P. E. Pidcoe, "The biomechanics principles behind training giant swings," Online, Virginia Commonwealth University, Richmond, VA, USA, August 2005, accessed 11 September 2020. <https://usagym.org/pages/home/publications/technique/2005/8/giant.pdf>.
- [2] V. Sevez, E. Berton, G. Rao, and R. J. Bootsma, "Regulation of pendulum length as a control mechanism in performing the backward giant circle in gymnastics," *Human Movement Science*, vol. 28, no. 2, pp. 250 – 262, March 2009.
- [3] J. Hauser and R. Murray, "Nonlinear controllers for non-integrable systems: the acrobot example," in *1990 American Control Conference*. San Diego, USA: IEEE, May 1990.
- [4] X. Wang, "Motion control of a gymnastics robot using virtual holonomic constraints," Master's thesis, University of Toronto, 2016.
- [5] E. Papadopoulos and G. Papadopoulos, "A novel energy pumping strategy for robotic swinging," in *2009 17th Mediterranean Conference on Control and Automation*. Thessaloniki, Greece: IEEE, June 2009.
- [6] T. Henmi, M. Chujo, Y. Ohta, and M. Deng, "Reproduction of swing-up and giant swing motion of acrobot based on a technique of the horizontal bar gymnast," in *Proceedings of the 11th World Congress on Intelligent Control and Automation*. Shenyang, China: IEEE, June 2014.
- [7] X. Zhang, H. Cheng, Y. Zhao, and B. Gao, "The dynamical servo control problem for the acrobot based on virtual constraints approach," in *The 2009 IEEE/RSJ International Conference on Intelligent Robots and Systems*. St. Louis, USA: IEEE, October 2009.
- [8] K. Ono, K. Yamamoto, and A. Imadu, "Control of giant swing motion of a two-link horizontal bar gymnastic robot," *Advanced Robotics*, vol. 15, no. 4, pp. 449 – 465, 2001.
- [9] T. Takubo, H. Arai, and K. Tanie, "Virtual nonholonomic constraint for human-robot cooperation in 3-d space," in *2000 IEEE/RSJ International Conference on Intelligent Robots and Systems*. Takamatsu, Japan: IEEE, October 2000.
- [10] S. Shibata and T. Murakami, "Psd based virtual nonholonomic constraint for human interaction of redundant manipulator," in *Proceedings of the 2004 IEEE International Conference on Control Applications*. Taipei, Taiwan: IEEE, September 2004.
- [11] J. D. Castro-Díaz, P. Sánchez-Sánchez, A. Gutiérrez-Giles, M. Arteaga-Pérez, and J. Pliego-Jiménez, "Experimental results for haptic interaction with virtual holonomic and nonholonomic constraints," *IEEE Access*, vol. 8, pp. 120959 – 120973, July 2020.
- [12] S. Vozar, Z. Chen, P. Kazanzides, and L. L. Whitcomb, "Preliminary study of virtual nonholonomic constraints for time-delayed teleoperation," in *2015 IEEE/RSJ International Conference on Intelligent Robots and Systems*. Hamburg, Germany: IEEE, October 2015.
- [13] B. Griffin and J. Grizzle, "Nonholonomic virtual constraints for dynamic walking," in *2015 54th IEEE Conference on Decision and Control*. Osaka, Japan: IEEE, December 2015.
- [14] J. Horn, A. Mohammadi, K. Hamed, and R. Gregg, "Hybrid zero dynamics of bipedal robots under nonholonomic virtual constraints," *IEEE Control Systems Letters*, vol. 3, no. 2, pp. 386 – 391, April 2019.
- [15] W. K. Chan, Y. Gu, and B. Yao, "Optimization of output functions with nonholonomic virtual constraints in underactuated bipedal walking control," in *2018 Annual American Control Conference*. Milwaukee, USA: IEEE, June 2018.
- [16] J. C. Horn, A. Mohammadi, K. A. Hamed, and R. D. Gregg, "Nonholonomic virtual constraint design for variable-incline bipedal robotic walking," *IEEE Robotics and Automation Letters*, vol. 5, pp. 3691 – 3698, February 2020.
- [17] R. D. Schafer, *An Introduction to Non-Associative Algebras*. New York: Dover Publications, 1996.
- [18] L. D. Landau and E. M. Lifschitz, *Mechanics*, 3rd ed. Butterworth-Heinemann, January 1982.
- [19] G. Golub and W. Kahan, "Calculating the singular values and pseudo-inverse of a matrix," *Journal of the Society for Industrial and Applied Mathematics: Series B, Numerical Analysis*, vol. 2, no. 2, pp. 204–224, 1965.
- [20] M. Maggiore and L. Consolini, "Virtual holonomic constraints for euler-lagrange systems," *IEEE Transactions on Automatic Control*, vol. 58, no. 4, pp. 1001 – 1008, April 2013.
- [21] S. Wirkus, R. Rand, and A. Ruina, "How to pump a swing," *The College Mathematics Journal*, vol. 29, no. 4, pp. 266 – 275, 1998.
- [22] N. Metropolis, "The beginning of the monte carlo method," *Los Alamos Science*, pp. 125–130, 1987, 1987 special issue dedicated to Stanislaw Ulam.